A&A 431, 1037–1046 (2005)
DOI: 10.1051/0004-6361:20048337

Astronomy & Astrophysics

On the origin of microwave zebra pattern

A. T. Altyntsev[1], A. A. Kuznetsov[1], N. S. Meshalkina[1], G. V. Rudenko[1], and Yihua Yan[2]

[1] Institute of Solar-Terrestrial Physics, Siberian Branch of the Russian Academy of Sciences, PO Box 4026, Irkutsk 33, 664033, Russia
e-mail: [altyntsev;a_kuzn]@iszf.irk.ru
[2] National Astronomical Observatories, Chinese Academy of Sciences, Datun Road A20, Chaoyang District, Beijing 100012, PR China
e-mail: yyh@bao.ac.cn

Received 24 May 2004 / Accepted 6 October 2004

Abstract. The results of the first observations of a zebra pattern at frequencies around 5.6 GHz are presented. The fine structures in the emission spectrum were recorded simultaneously by the Siberian Solar Radiotelescope and the spectropolarimeters of the National Astronomical Observatories, which allowed us to study the presented event with high spatial, temporal and spectral resolution. The apparent source size does not exceed 10 arcsec, and the sources of the different stripes of the zebra structure coincide spatially. The circular polarization degree reaches 100%, and the polarization sense corresponds to the extraordinary wave. We argue that the most probable generation mechanism of the zebra pattern is nonlinear coupling of Bernstein waves. In this case the value of the magnetic field in the burst source, determined by the frequency separation between the adjacent stripes, is 60–80 G.

Key words. radiation mechanisms: non-thermal – Sun: flares – Sun: radio radiation

1. Introduction

Observations of radio bursts with zebra-like fine spectral structure, seen as a number of parallel bright stripes in the dynamic spectrum, give an unique means for the local measurement of magnetic field values in the solar corona. In the meter and decimeter waves, bursts with zebra structures are observed rather frequently during solar flares. In the microwave range such events are more rare; their observations have become available with the spectropolarimeters of the National Astronomical Observatories (Huairou station) (Fu et al. 1995). Until now, the highest frequency at which a zebra pattern has been observed is 3.8 GHz (Chernov et al. 2001, 2003).

There are several approaches to the interpretation of bursts with zebra-like fine structure, which were developed with reference to the bursts in the meter and decimeter ranges. The physical mechanisms can be subdivided into two categories. For the first it is suggested that all stripes of the zebra pattern are generated in the same source, whereas in the other models different stripes are emitted by different sources, separated spatially. The first group of models assumes simultaneous generation of several cyclotron harmonics in the same source. In this case the electromagnetic emission arises due to nonlinear coupling of Bernstein waves with each other or with upper-hybrid plasma waves (Rosenberg 1972; Chiuderi et al. 1973; Zheleznyakov & Zlotnik 1975a, 1975b; Mollwo & Sauer 1977; Zaitsev & Stepanov 1983). The generation of several cyclotron harmonics of upper-hybrid waves with the subsequent conversion into radio emission was suggested also by Winglee & Dulk (1986). In these models the frequency separation between the adjacent stripes is close to the electron cyclotron frequency.

The other group of models explains the zebra structure by emission from different sites on the magnetic loop, where some resonant conditions are fulfilled. In particular, the generation of upper-hybrid waves on the surfaces of double plasma resonance (Kuijpers 1975; Zheleznyakov & Zlotnik 1975b; Ledenev et al. 2001) and coupling of plasma waves and whistlers (Chernov 1976, 1990) are considered. LaBelle et al. (2003) have proposed a model where the discrete spectrum of upper-hybrid waves arises due to their trapping by plasma microinhomogeneities. For these models the frequency interval between the zebra stripes can differ considerably from the electron cyclotron frequency.

In the present paper we describe the results of the first observations of zebra patterns in the centimeter range, which combine high spatial, spectral and temporal resolution.

2. Observation techniques

The dynamic spectra of the zebra structures were observed with the Solar Radio Broadband Fast Dynamic Spectrometers (5.2–7.6 GHz) at the Huairou Solar Observing Station of the National Astronomical Observatories of China (NAOC) (Fu et al. 1995). The receiving band of one frequency channel of the NAOC spectropolarimeter is 20 MHz, and the temporal resolution is 5.9 ms (Ji et al. 2003).

The spatial characteristics of the microwave sources were recorded by the Siberian Solar Radiotelescope (SSRT) (Smolkov et al. 1986; Grechnev et al. 2003). The SSRT is a crossed radio interferometer, consisting of two lines of antennae, in the east-west (EW) and the north-south (NS) directions, operating in the 5.67−5.79 GHz frequency range. Radio maps of the solar disk are recorded at intervals of 3−5 min. The investigations of fine temporal structure of the flare bursts are based on the data recorded by the EW and NS arrays, which simultaneously provide one-dimensional images (scans) of the solar disk every 14 ms.

The investigation methods for one-dimensional solar images have been described by Altyntsev et al. (1996, 2003). The SSRT receiving system contains a spectrum analyser in the 120 MHz frequency band, represented by an acousto-optic receiver, featuring 250 frequency channels, which correspond to the fans of knife-edge beams for the NS and EW arrays, respectively. The frequency channel bandwidth is 0.52 MHz. The response at each frequency corresponds to the emission from the narrow band on the solar disk whose position and width depend on the observation time, the array type and on the frequency. The signals from all the channels are recorded simultaneously and generate a one-dimensional distribution of the solar radio brightness. The components of circular polarization (right and left) are recorded successively within intervals of 7 ms duration each.

The SSRT beam minimal width is 15 arcsec, and depends on the array direction and the observation local time. The burst with zebra structures was detected near local noon, when the solar disk was being observed by the NS interferometer in two orders simultaneously. In this case the solar microwave sources were recorded simultaneously in two narrow frequency bands within the SSRT receiving band. On the other hand, the spatial resolution of the NS array was insufficient around noon for studying the internal structure of the flare microwave sources, as the beam half width was about 50.1 arcsec at that time, and the angular distance between the adjacent channel beams was 54.3 arcsec. The direction of NS scanning was −58.3 degrees to the central solar meridian. The observation conditions for the EW array differed considerably. The scanning direction was −4.7 degrees, the beam half width was 16 arcsec, and the angular distance between the directions of the adjacent frequency channels was 3.8 arcsec. Due to the small size of the flare microwave bursts, they are recorded by the SSRT in the narrow band not exceeding 5 MHz.

To study the dynamics of the microwave burst spectrum in the 2.0−35 GHz range, the data from the Nobeyama spectropolarimeters were used. The flare structure was defined using the SOHO/EIT images in the soft ultraviolet radiation. The magnetic field structure was determined using the SOHO/MDI magnetograms.

3. Observations

3.1. The temporal profiles

The microwave burst with zebra structures was observed during the flare on January 05, 2003 (C5.8/SF 0617 UT), in the AR 0243 (S20W51) active region. The temporal profiles of the microwave emission are presented in Fig. 1. At 5.7 GHz the temporal profile was obtained from the NAOC data. The magnitude calibration at this frequency was made applying the SSRT data. It is evident that the spike-like pulses with duration of several seconds were observed at the frequencies below 5.7 GHz. At 3.8 GHz the right-hand polarized pulses were registered for 12 min. Note the absence of pulse-pulse correlation between the signals at 2 and 3.8 GHz.

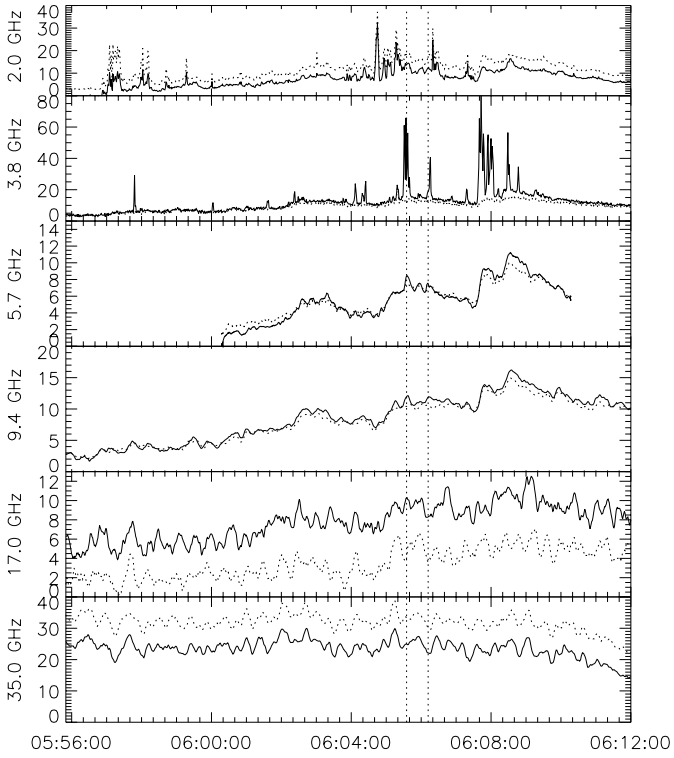

Fig. 1. The microwave fluxes of right (continuous curve) and left (dot curve) handed circular polarization, recorded by the Nobeyama spectropolarimeters at 2.0, 3.8, 9.4, 17.0, 35.0 GHz, and by the Huairou spectropolarimeters at 5.7 GHz. The flux magnitude is in sfu. The vertical dotted lines mark the zebra emission intervals (06:05:35 and 06:06:11 UT).

The moments of recording the zebra structures at 5.7 GHz are marked by the vertical lines. Zebra structures were observed three minutes prior to the background burst maximum. There are three flux fluctuations with a duration of 170 s during the gradual growth of the background emission at 5.7 GHz. The flux spectrum of the background burst at the moments of zebra recording is flat at frequencies lower than 5.7 GHz, and decreases at frequencies over 9.4 GHz. The polarization degree of the background burst is low. Zebra patterns were observed close to the soft X-ray maximum (at 06:06 UT), when the GOES fluxes were 5.15×10^{-6} W m^{-2} for 1−8 Å, and 5.62×10^{-7} W m^{-2} for 0.5−4 Å.

The dynamic spectra with zebra structures are shown in Figs. 2, 3 along with the SSRT time profiles. Zebra patterns are clearly visible in the original NAOC dynamic spectra. However, for a more accurate determination of the burst parameters, we performed background subtraction. The "sliding window" algorithm was used, when the background level in

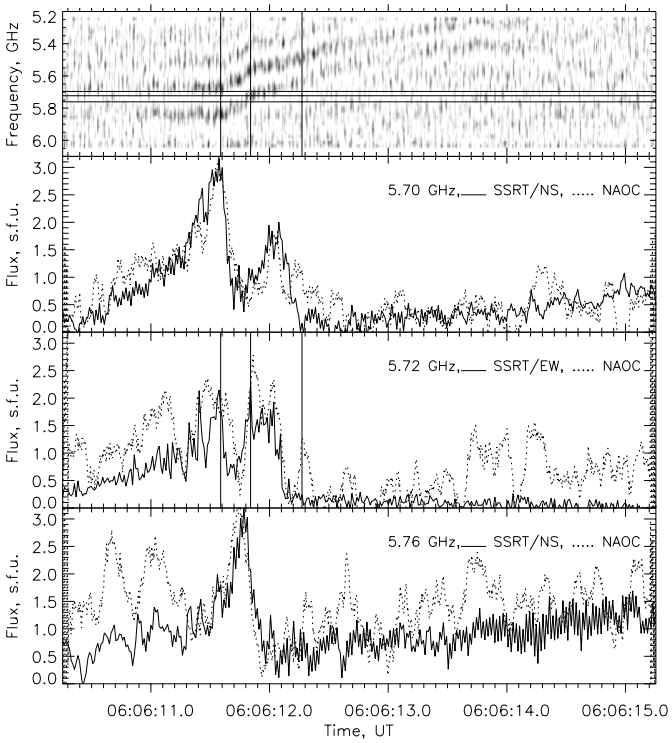

Fig. 2. Zebra pattern at 06:06:11 UT. *Top*: the NAOC dynamic spectrum. Darker areas correspond to the higher intensity of emission. The horizontal lines show the frequencies recorded by the SSRT linear interferometers. The vertical lines mark the moments of the one dimensional images in Fig. 6. *Bottom*: the temporal profiles, recorded by the NAOC spectropolarimeters and the SSRT linear arrays at the same frequencies.

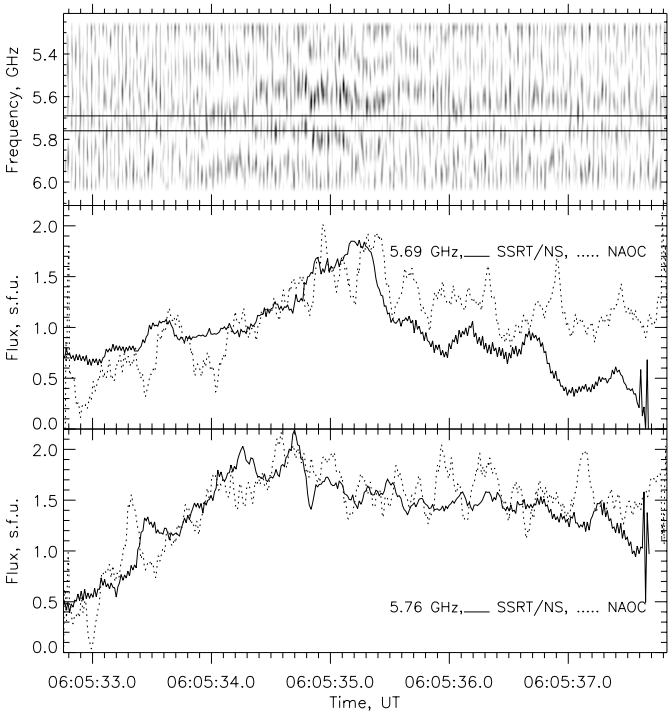

Fig. 3. The same as in Fig. 2 for the zebra pattern at 06:05:35 UT.

each point is determined as the average flux in the 7×7 points (or 41.3 ms $\times$ 140 MHz) rectangle. Sometimes in the gaps between the bright stripes this procedure results in negative values that have been cut off (replaced by zero) for better edge sharpening. For the SSRT time profiles we subtracted the constant background value, which was determined as the flux value in some moment prior to the zebra-like burst.

The brighter zebra pattern appeared after 06:06:10.3 UT (Fig. 2). Its dynamic spectrum consists of three bright stripes. The burst spectrum has a U-like form; the first half is brighter, the other is less so. The duration of the increasing (first) branch of the burst is about 2.5 s, the other branch about 2 s. Near the turnover point the low-frequency stripe goes out of the receiver range. There is a fourth, weaker stripe, before the drift start at low frequency. The mean frequency of the event can be estimated as 5.6 GHz. The frequencies of separate zebra stripes vary in the intervals of 5.86−5.40 GHz, 5.70−5.30 GHz and 5.54−(about 5.2) GHz; the frequency interval between adjacent stripes has an almost constant value of 0.16 GHz. The relative frequency change during the zebra pattern is about 8%. The drift rate is -0.7 GHz s^{-1} at the beginning, then it reduces gradually to zero, and reaches $+0.45$ GHz s^{-1} during the second branch of the burst. The instantaneous bandwidth of the stripes is about 0.06 GHz. We can see that all the zebra stripes start their drift simultaneously, with an accuracy of 50 ms.

The weak absorption between the bright stripes is observed in the instant spectra. The zebra structure has been recorded by both instruments in the right handed mode only. Thus, the circular polarization degree of the zebra pattern reaches 100%.

In Fig. 3 another case of zebra structure is shown. In this case there is no frequency drift. It is possible to distinguish up to four bright stripes with a frequency separation of 0.22 GHz. At the moment of that zebra structure the emission source was observed only by the NS interferometer.

The bottom panels in Figs. 2 and 3 show a satisfactory correspondence between the SSRT and NAOC temporal structures at the same frequencies. This demonstrates the solar origin of the spectral structure. The SSRT temporal profiles have been calculated from the sequences of the zebra source one-dimensional images. The flux of zebra stripes reaches 3 sfu. The flux plot at a single frequency shows a sawtooth behavior: an exponential growth with a scale of 0.5 s, and an abrupt decrease with time by an order less.

3.2. Spatial structure of flare

The magnetogram of the flare region is shown in Fig. 4. The magnetic field structure can be classified as $\beta\gamma/\beta$. The magnitude of the field in the leading spot of the S-polarity reaches 875 G; the spot of the N-polarity is displaced 45 arcsec to the north-east. The contours in Fig. 4 show the emission brightness in the UV (195 Å) at the flare peak. The UV contours show a loop connecting the two sites with the magnetic fields of opposite direction (sources 1 and 2). The distance between them is about 35 arcsec. The crossing of the direct lines points to the brightness centroid of the zebra source, which is located

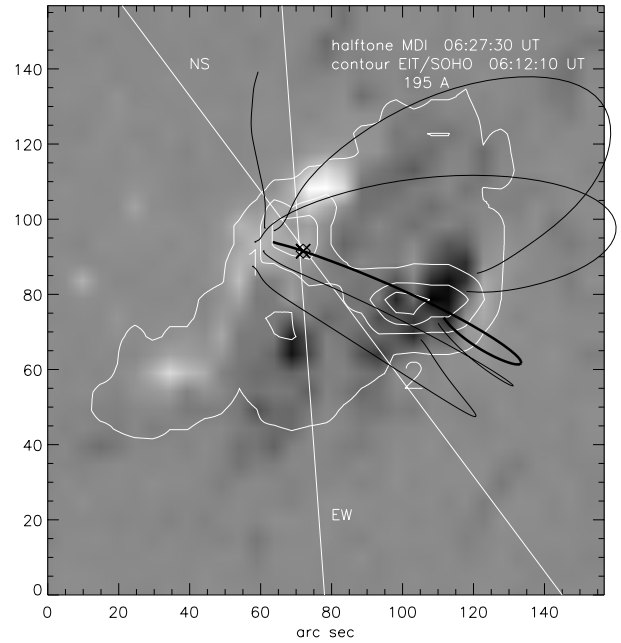

Fig. 4. The magnetogram (halftone) and the UV emission map (contour) of the AR 0243 flaring region. The crossed straight lines show the scanning directions of the EW and NS linear interferometers. The intersection point corresponds to the position of the zebra source. The contour levels are 45%, 60%, 75% and 90% of the maximum values.

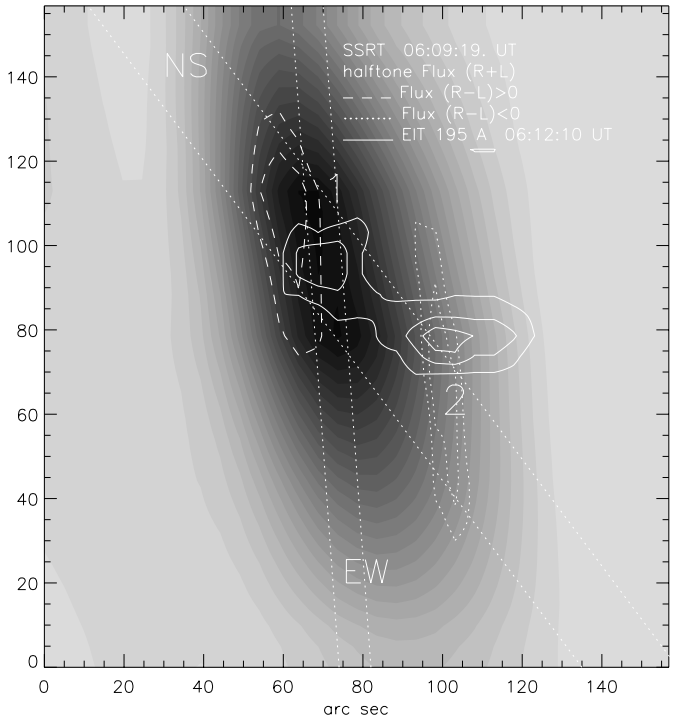

Fig. 5. The structure of the microwave emission at 5.7 GHz. The brightness temperature in intensity ($R + L$) is shown by grayscale. The maximum value is 2.7×10^6 K. The dashed lines correspond to the contours in polarization ($R-L$) with the levels 80% and 90% of the maximum values. The maximum values are 7×10^5 K and -1.2×10^5 K, respectively. The straight dashed lines mark the bands on the solar disk, the emission from which is recorded during the zebra pattern observation. The solid contours show the UV emission, and are the same as in Fig. 4.

near the north-east loop foot, where the magnetic field value (at the photosphere) is about 150 G of the N-polarity (source 1).

The structure of the microwave sources at 5.7 GHz is shown in Fig. 5. There is a correspondence of sources 1 and 2 with the sources with the right and left polarization, accordingly. The polarization degrees reach +28% and −10%. The brightness center of the background flare burst is close to source 1. Before the flare, the polarization centers were not visible. The flare source 2 became visible at 05:50 UT. Source 1 appeared later, at 06:00 UT, and it became brighter than source 2 about 10 min later. The same structure of the background burst is seen in the NoRH radio maps at 17 GHz.

The straight dashed lines define the bands around the straight lines shown in Fig. 4. Their widths equal the half widths of the corresponding interferometer beams, and can be considered as the upper estimate of the error in the source location. Thus, the zebra source is located within the parallelogram formed by the direct dashed lines. The overlap with the magnetogram shows that the magnetic field inside the parallelogram has N-polarity.

In Fig. 6 the one-dimensional distributions of the background burst radio brightness (scans), recorded by the EW array, are shown in intensity and polarization. The positions of 130 and 165 arcsec here correspond to the loop footpoints, and one can see different polarization signs at these points. The scans of the zebra source are shown for the two consecutive moments corresponding to the different stripes. It is evident that the locations of different stripe sources coincide, and they are displaced a few arcsec to the east of the background burst brightness center. The zebra source is significantly smaller than the background burst source, and its width is less than 20 arcsec. The width of the corresponding SSRT beam is close to 16 arcsec. So, taking into account this beam width, we can estimate the zebra source apparent size as less than 10 arcsec, or 7 thousand km.

4. Discussion

4.1. The plasma parameters in the emission source

SOHO/MDI and SOHO/EIT observations show that the main microwave source is located near the loop footpoint, in the region of the magnetic field with N-polarity and a strength of about 150 G. The distance between the loop footpoints is 35 arcsec, or more than 25 thousand km in the image plane.

The polarized radio sources at the frequencies of 5.7 and 17 GHz are observed near the loop footpoints. The source of the right-handed circular polarization corresponds to the northern polarity footpoint, and the opposite polarization at the other footpoint. This means that the loop footpoints are the sources of the extraordinary mode of the electromagnetic radiation.

The wave mode of the footpoint emission and dependence of the background microwave spectrum on the frequency suggests a gyrosynchrotron emission mechanism. Assuming a power-law energy distribution of the emitting electrons

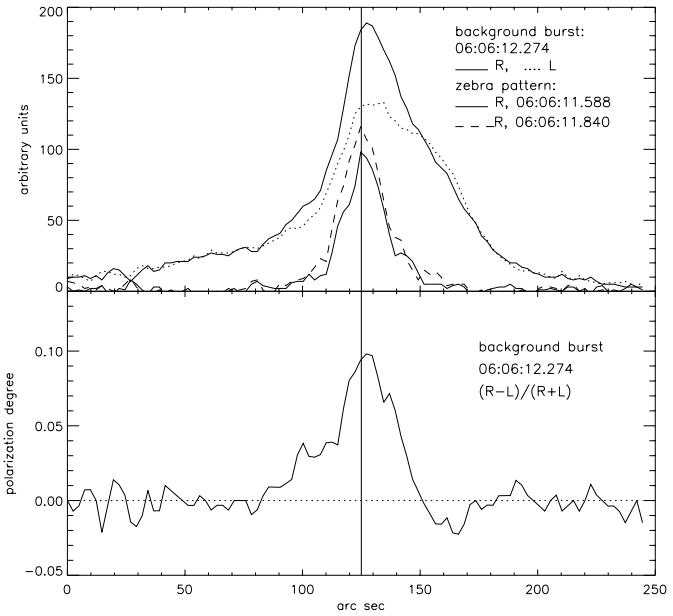

Fig. 6. The one-dimensional distributions of the microwave emission (scans) and polarization degree, recorded by the EW array. The scans of the background burst in the right and left handed polarization are shown in the upper panel, and the polarization degree is presented in the bottom. The zebra scans are obtained by subtracting the background scan from the scans, corresponding to the zebra brightening.

(Dulk 1985) we can estimate the power-law index as 3.16, using the observed ratio of the flux values at 9.4 and 17 GHz.

The ratio of the GOES signals (1–8 Å and 0.5–4 Å) allows us to estimate the plasma temperature in the flaring loop as 1.1×10^7 K. The estimation of the integral emission measure from the flux values is $n^2V \simeq 6.4\times10^{48}$ cm^{-3}. If one assumes that the emission region volume is determined by the loop dimensions in the UV emission in Fig. 4, then this volume is estimated as $V \simeq$ (25 thousand km) $\times$ (7 thousand km)$^2 = 1.2\times10^{27}$ cm^3. So, the estimation of the plasma density is $n \simeq 7.2\times10^{10}$ cm^{-3}.

It will be shown in Sect. 4.4 that the model of nonlinear interaction of Bernstein waves is the most suitable to explain the polarization, spectral and temporal parameters of the observed zebra pattern. In this case the frequency interval between adjacent bright stripes is almost equal to the electron cyclotron frequency $\Delta\nu = \dfrac{eB}{2\pi mc}$ in the emission source. Therefore the observations of a zebra pattern provide a direct method for magnetic field magnitude measurement. In the event under consideration, we managed to detect the zebra patterns twice with frequency intervals of 220 and 160 MHz, respectively. These values correspond to the magnetic field strength B of 60–80 G in the zebra source.

Note that for zebra bursts in metric and decimetric ranges the mechanisms that connect the frequency separation of zebra stripes directly to the electron cyclotron frequency sometimes give unrealistically small values of the magnetic field, and therefore were ruled out by many authors. But in the event under consideration the obtained magnetic field corresponds well to the results of magnetic field modeling. Also, this estimation does not conflict with the characteristics of the background gyrosynchrotron source (namely, the spectrum shape and polarization degree).

In Fig. 4 we show the magnetic field lines, calculated in the potential field approximation using the MDI magnetogram. The calculation method was developed by Rudenko et al. (1998). Adjustment of the scales and positions on the solar disk was made using the code of Rudenko & Grechnev (1999). One of the magnetic lines connecting sources 1 and 2 is marked by the thick line in Fig. 4. Its length is 130 thousand kilometers and its height is about 45 thousand kilometers. It is remarkable that the point of this line with the magnetic field value of 60 G is close to the visible position of the zebra source. So, we believe that this site, marked by the cross in Fig. 4, corresponds to the zebra source location. The height of this point above the photosphere is about 14 thousand kilometers.

The zebra pattern emission can be explained by coherent emission processes due to the narrow bandwidth of the instant spectrum. In the centimeter range a coherent emission is generated mainly at the frequencies near the double Langmuir frequency. When the plasma density is 7.2×10^{10} cm^{-3}, the double Langmuir frequency equals 4.8 GHz and this value agrees with the observations of the fine temporal structures at frequencies 3.8–5.7 GHz during the flare under consideration.

Unlike the zebra pattern, the background burst is generated in a more extended region inside which the plasma density can vary considerably. The peculiarity of the event under study is the unusually low value of the background spectrum turnover frequency (>2 GHz). So, we can conclude that the emission is not suppressed by the Razin effect at frequencies down to 2 GHz. This effect is important at the frequencies below $\nu_c = 20n/B$ (Dulk 1985). Assuming $\nu_c = 1$ GHz and $B = 60$ G we get an upper estimation for the plasma density in the background gyrosynchrotron source as 3×10^9 cm^{-3}. This value is considerably smaller than the value obtained from the GOES signals. It seems that the flare region is a mixture of thin dense tubes and transparent ones. The dense tubes emit UV and microwave coherent emission and the others produce the gyrosynchrotron emission.

The upper limit of the zebra source size in the image plane can be estimated as 10 arcsec (Fig. 6). The real size can be smaller because the apparent size can be significantly overestimated due to emission scattering by the density inhomogeneities in the low solar corona. Due to this effect the apparent size of the subsecond pulse sources increases for the events at high longitudes. For the sources at longitude 51 degrees the increase is about 10 arcsec (Altyntsev et al. 1996, Fig. 3). The transversal source size $r_\perp$ can be estimated with the assumption that the zebra pattern frequency drift is caused by the tube radial expansion with the Alfvén velocity, $r_\perp \simeq v_A\Delta t$. For the brightest zebra event (in Fig. 2) $\Delta t \simeq 2.5$ s and we get the source size of about one thousand km.

Note that the apparent positions of the sources of two different stripes of the zebra pattern coincide. The frequency drift starts simultaneously at all the zebra stripes, which confirms the conclusion that different stripes are generated in the same source. The stripes with higher frequency are brighter, which can be explained by the lesser absorption of the emission in the plasma outside the source. The absorption optical

depth is $\tau \simeq 46\, T^{-3/2}\nu^2 L_\mathrm{p}$ for the emission near the fundamental plasma frequency and $\tau \simeq 1.2\, T^{-3/2}\nu^2 L_\mathrm{p}$ near the second harmonic (T is temperature in K, ν is frequency in GHz, L_p is the plasma density inhomogeneity scale in the direction of the emission propagation, in cm) (Benz et al. 1992). When $T = 1.1 \times 10^7$ K, $\nu = 5.6$ GHz and $\tau = 1{-}2$, we obtain the required inhomogeneity scale $L_\mathrm{p} = 250{-}500$ km for the fundamental emission and $L_\mathrm{p} = 9.7{-}19.4$ thousand km for the harmonic emission. Therefore, we can conclude that the escape of emission at the frequency near the fundamental one is ineffective and unlikely.

4.2. Flare loop oscillations

It has been already noted that the synchronous intensity oscillations with a 170 s period were observed at all the ranges of the background burst microwave emission. This phenomenon can be explained by the modulation of the magnetic field strength and loop size due to oscillations with a period depending on loop length. The TRACE observations show flare-induced impulsively generated MHD waves, which propagate back and forth in the loop (Schrijver et al. 2002; Aschwanden et al. 2002). In this case the oscillation period can be estimated as $\tau \simeq 2L/\langle v_\mathrm{A}\rangle$, where L is the loop length, and $\langle v_\mathrm{A}\rangle$ is the mean Alfvén velocity along the loop,

$$\langle v_\mathrm{A}\rangle = \frac{1}{L}\int_0^L v_\mathrm{A}(l)\mathrm{d}l. \quad (1)$$

We must use the mean velocity because of the strong dependence of the magnetic field in a coronal loop on height.

To estimate the oscillation period we have used the properties of the thick magnetic line in Fig. 4. We have found that the magnetic field varies from 500−800 G in the loop footpoints down to 20 G in the loop apex. For the plasma density 3×10^9 cm^{-3} we have found that the mean Alfvén velocity $\langle v_\mathrm{A}\rangle = 1430$ km s^{-1}, and the oscillation period $\tau \simeq 180$ s. This result does not change considerably if we take into account the barometric dependence of the plasma density for a loop temperature of 10^7 K. So, the calculated period is in good agreement with the observed one if the plasma density value is taken from the estimations based on the properties of the background burst microwave spectrum.

4.3. The wave mode of the zebra pattern

It has already been noted that the zebra emission has 100-percent circular right-hand directed polarization. The magnetic field in the parallelogram around the possible zebra source locations (see Fig. 5) has N-polarity, which corresponds to the extraordinary wave (X-mode). The results of the magnetic field interpolation to the corona confirm this conclusion. An error in the mode determining can occur if: a) the magnetic field in the loop dramatically differs from the field, calculated with the potential approximation, and the magnetic field direction at the source height is opposite to the magnetic field in the photosphere; b) there is a tiny region with the reverse direction of the magnetic field, which is not resolved in the magnetogram and the zebra pattern is generated above this region. Both these assumptions are unlikely due to the magnetic field structure in the given event: the magnetic configuration is not complex, the height of the source above the photosphere does not exceed 15 thousand km. Also, the zebra pattern polarization sign is the same as the gyrosynchrotron background emission sign, which is polarized in the extraordinary sense at the SSRT receiving frequency.

At present, the opinion is widespread that, in the meter and decimeter ranges, the zebra pattern polarization corresponds to the ordinary wave (O-mode) (Chernov et al. 1975, 1994; Zlobec et al. 1987; Chernov & Zlobec 1995). In this article the observations show the opposite polarization. Possibly, the zebra origin at low and high frequencies is different.

On the other hand, we believe that the wave mode of the meter and decimeter zebra bursts has not been unambiguously determined yet. There were few observations with direct source localization on the solar disk. In most cases the source positions were determined by indirect methods (for example, from the position of the corresponding optical flare). Meter and decimeter bursts are generated at rather large altitudes, where the photospheric magnetic field extrapolation is not sufficiently reliable. In addition, in some of the above cited papers the flares with zebra patterns were observed in rather complex configurations of the magnetic field.

4.4. The zebra pattern generation mechanism

The determination of the zebra pattern generation mechanism is nesessary in order to utilize the diagnostic potential of such bursts. Also, such an investigation can help us better understand the origin of other types of solar radio emission with similar features. For example, Chernov et al. (2003) have found that the zebra stripes often have a fine temporal structure and consist of separate spike-like pulses. On the other hand, the millisecond spikes sometimes demonstrate a quasiharmonic spectral structure with simultaneous emission generation at several frequencies (see the review of Fleishman & Melnikov 1998). We will now examine the processes that can lead to forming a zebra pattern in the dynamic spectrum.

The coalescense of Bernstein modes with upper-hybrid waves. This mechanism was proposed first to explain the zebra bursts (Rosenberg 1972; Chiuderi et al. 1973; Zheleznyakov & Zlotnik 1975b). The electromagnetic emission arises due to the process of nonlinear coupling of upper-hybrid plasma waves with the frequency $\nu_\mathrm{uh} = \sqrt{\nu_\mathrm{p}^2 + \nu_\mathrm{B}^2} \simeq \nu_\mathrm{p}$ and Bernstein modes with the frequency close to harmonics of the electron cyclotron frequency, $\nu_\mathrm{Ber} \simeq s\nu_\mathrm{B}$ (ν_B and ν_p are electron cyclotron and Langmuir frequencies). Thus, the emission is generated at the frequencies $\nu \simeq \nu_\mathrm{p} + s\nu_\mathrm{B}$, and the frequency interval between adjacent zebra stripes equals the electron cyclotron frequency. Bernstein modes and upper-hybrid waves are both effectively generated by an anisotropic electron distribution of a loss-cone type (Zheleznyakov & Zlotnik 1975a), and increments of the different harmonics of Bernstein modes

are comparable. Numerical calculations show that if the energy of the accelerated electrons is not too low ($T_h/T_0 > 4$) then generation of the harmonics with $\nu_{Ber} < \nu_p$ and the frequency just below $s\nu_B$ is most effective (Willes & Robinson 1996). Therefore, the emission frequency lies between ν_p and $2\nu_p$. Both Bernstein modes and upper-hybrid waves propagate almost perpendicularly to the magnetic field and have comparable wave vector values $k_\perp$, so the kinematic conditions of the coalescence are satisfied.

The polarization of emission resulting from this process corresponds to the ordinary wave (Zlotnik 1977), its degree depends on the angle α between the propagation direction and the magnetic field vector as $r = 2\cos\alpha/(1+\cos^2\alpha)$, and can be as high as 100%. Nevertheless, the polarization sign does not correpond to our observations. Another shortcoming of the mechanism is that the increment of the upper-hybrid waves significantly (by one-two orders of magnitude) exceeds the increment of Bernstein modes (Zheleznyakov & Zlotnik 1975a). Consequently, the unstable electron beam will amplify mainly upper-hybrid waves, and the energy density of Bernstein modes will be too low to provide the observable intensity of radio emission.

The coalescence of Bernstein modes. In this process the nonlinear coupling of different harmonics takes place, $\nu = s_1\nu_B + s_2\nu_B$ (Zheleznyakov & Zlotnik 1975b; Mollwo & Sauer 1977). To provide sufficient energy density of the Bernstein modes, the generation of upper-hybrid waves must be suppressed. Upper-hybrid waves (plasma waves with a normal dispersion law) at the sth harmonic are generated if the energy of the accelerated particles exceeds the value (Zheleznyakov & Zlotnik 1975a):

$$\frac{T_h}{T_0} > s, \tag{2}$$

where T_h and T_0 are the effective temperatures of the accelerated particles and background plasma. If the condition is not satisfied, one can expect the growth of several modes with an anomalous dispersion law, with comparable parameters (wave vectors and increments) at the frequencies close to the electron cyclotron harmonics.

The frequency interval between adjacent zebra stripes equals $2\nu_B$ if only the plasma waves with the same harmonic number s participate in the coupling process, and it equals ν_B if the coupling of different harmonics is possible. Let us consider the conditions of the adjacent mode interaction, $s_2 = s_1 + 1$. The kinematic conditions require that the coupling longitudinal waves be almost oppositely directed, and their wave vectors be comparable, or $|k_{\perp 2} - k_{\perp 1}| < 2\pi\nu/c$, where $2\pi\nu/c$ is the wave vector of the electromagnetic wave. As Bernstein modes propagate perpendicularly to the magnetic field, it is possible for each wave to find the oppositely directed wave. The wave vector value depends on the energy (to be more exact, on the transversal component of the velocity $v_\perp$) of the emitting electrons as (Winglee & Dulk 1986)

$$k_\perp \simeq \frac{2\pi s\nu_B}{v_\perp}. \tag{3}$$

Consequently, the kinematic conditions for the adjacent mode coupling at $s \gg 1$ are satisfied, if

$$\frac{v_\perp}{c} > \frac{\nu_B}{\nu}. \tag{4}$$

From the observations we have $\Delta\nu/\nu = 1/35$, and the Eq. (4) reveals the energy of the accelerated electrons $E > 210$ eV. In flares the electron beams have significantly higher energy, so one can expect the interaction between the different harmonics of Bernstein modes, and the frequency interval between the zebra pattern adjacent stripes equals the electron cyclotron frequency ν_B. The emission frequency lies in the interval between the fundamental plasma frequency and its harmonic (more accurate estimation requires the calculation of the energy spectrum of Bernstein modes for the given unstable electron distribution).

In this case the polarization corresponds to the extraordinary wave (Mollwo & Sauer 1977). The numerical modeling carried out by Haruki & Sakai (2001) shows that the polarization degree of the electromagnetic waves (in the X-mode sense) can reach 100% for coupling of Bernstein modes. The investigation by Willes (1999) shows that the efficiency of the nonlinear interaction is sufficient to provide radio emission with the observed intensity; it is also shown that the polarization sign depends on the specific conditions, but in most cases it corresponds to the extraordinary wave. The polarization degree can be up to 60% in the X-mode sense. Therefore, we can conclude that the interpretation on the basis of the nonlinear coalescence of Bernstein modes agrees well with our observations. However, an additional investigation is required to find out the relation between the high degree of polarization with the emission source parameters (in particular, with the parameters of the unstable electron distribution).

The observed ratio of the emission frequency to the frequency interval between the zebra pattern stripes is about 35, which corresponds to the generation of the plasma waves with harmonic numbers of about 17−18. The increase in number of the generated harmonics with the increase of the emission frequency (and the density of the coronal plasma) was first noticed by Güdel (1990). According to his observations, the emission in the decimeter range can be associated with the generation of the electrostatic waves with harmonic numbers of about 6 (possibly, up to 8). Our observations show that this tendency of increasing harmonic numbers remains valid in the microwave range.

The generation of several cyclotron harmonics of upper-hybrid waves. This model was proposed first in the paper of Winglee & Dulk (1986). Unlike in the previous mechanism, the condition (2) is considered to be satisfied. In plasma with a nonzero temperature the upper-hybrid waves frequency can differ from ν_{uh}. If the distribution function of the nonthermal electrons has a positive slope in a sufficiently broad range of velocities $v_\perp$, then the condition for the generation of the longitudinal waves (3) can be satisfied for more than one harmonic number s; this requires the electron distribution of a hollow beam type or loss-cone with a smooth edge. Then the plasma waves are transformed into radio emission due to nonlinear

processes. It has been noted above that the conditions of the emission escaping from the corona make the emission generation at frequencies close to the plasma one unlikely. The process of two plasma wave coupling is more effective. Coupling of the different cyclotron harmonics of upper-hybrid waves requires the same condition (4) as for Bernstein modes, but the dispersion equation of upper-hybrid waves results in the additional limitation on the plasma temperature from below: $v_T^2 > cv_\perp/(6s)$, where v_T is the mean thermal velocity of the background plasma electrons, $v_\perp$ is a transversal component of the accelerated electron velocity. For the electron energy of 20 keV and $s = 20$ we obtain $T > 7 \times 10^6$ K, which is satisfied in the burst source under consideration. Therefore, the frequency interval between adjacent zebra stripes will be equal to the electron cyclotron frequency ν_B, as in the two previous mechanisms.

The polarization of the electromagnetic emission, arising due to coupling of upper-hybrid waves, corresponds to the extraordinary wave and the polarization degree is $r = -1.7(\nu_B/\nu_p)\cos\alpha$ (Zlotnik 1981). If $\nu_B/\nu_p = 1/35$, then the polarization degree does not exceed 5%, which does not correspond to the high degree observed. Also, it is not easy to obtain comparable emission intensities in the different stripes by that mechanism. The calculations show that the increments of harmonics depend strongly on the ratio ν_p/ν_B, and a small change in that ratio (no more than 1%) can result in an essential change of the burst structure.

The generation of upper-hybrid waves at the surfaces of the double plasma resonance. In this mechanism it is assumed that different zebra stripes are generated in different sources (Kuijpers 1975; Zheleznyakov & Zlotnik 1975b; Ledenev at al. 2001; Sawant et al. 2002; Aurass et al. 2003; Zlotnik et al. 2003; Yasnov & Karlicky 2004) where the double plasma resonance condition is satisfied: the upper-hybrid frequency is close to the harmonic of the electron cyclotron frequency, $\nu_{uh} \simeq \nu_p \simeq s\nu_B$. In contrast to the previous model, only one harmonic is generated due to the cyclotron resonance. The condition is satisfied if the distribution function of the accelerated electrons has a positive slope only in a quite narrow velocity range, or if the plasma temperature is relatively low (when upper-hybrid waves turn into Z-mode). The inequality (2) must be satisfied, otherwise the increment of upper-hybrid waves decreases radically.

In an inhomogeneous medium, if the inhomogeneity scales of ν_p and of ν_B are different, the double plasma resonance condition can be satisfied at different harmonic numbers s in the different points of the magnetic loop, and, consequently, for different frequencies of the generated waves. If the inhomogeneity scales of the magnetic field and the plasma density are $L_B = B/(\partial B/\partial r)$ and $L_p = n/(\partial n/\partial r)$, respectively, then the distance between the points of the generation of the upper-hybrid waves at the harmonics s and $s + 1$ is

$$\Delta r \simeq \frac{2L_pL_B}{sL_B - 2(s+1)L_p}, \tag{5}$$

and the frequency interval between adjacent zebra stripes is

$$\frac{\Delta\nu}{\nu} \simeq \frac{L_B}{sL_B - 2(s+1)L_p}. \tag{6}$$

These formulae are obtained under the assumption that $\nu_p \gg \nu_B$, and the radio emission frequency equals the frequency of upper-hybrid waves or their harmonic. Note that the frequency interval between the zebra stripes is not directly related to the cyclotron or plasma frequencies in the source.

The spatial parameters of the observed microwave zebra pattern do not rule out the described generation model. Although we do not see the difference of source positions of zebra stripes (Fig. 6), the set of double resonance sites can be observed along the direction of gradients of plasma density and magnetic field, and therefore the visible source positions coincide. Also, the spatial resolution can be insufficient to distinguish the double resonance layers. But, in our opinion, the main shortcoming of this model is its difficulty in explaining the observed parallel frequency drift of zebra pattern stripes.

Let us assume that the magnetic field inhomogeneity scale is about the coronal loop dimensions, $L_B = 10$ thousand km, $\Delta\nu/\nu = 1/35$, and $s = 10$ (that corresponds to $B = 100$ G if the emission is generated at the double upper-hybrid frequency). From formulae (5, 6) we obtain $L_p = 11\,350$ km and $\Delta r = 1520$ km. The MHD disturbance will pass this distance with the Alfvén velocity in the time interval $\Delta t \simeq \Delta r/v_A = 2.4$ s ($n = 10^{11}$ cm^{-3}). If $s = 5$ ($B = 200$ G), we obtain respectively $L_p = 25\,000$ km, $\Delta r = 2000$ km and $\Delta t = 1.5$ s. At the same time, as we have already noted, the zebra stripes show similarity in temporal evolution, with an accuracy not worse than 50 ms. To provide such temporal characteristics, a more compact emission source is required, and the inhomogeneity scales of the plasma and magnetic field must be much smaller than the coronal loop dimensions. As it can be seen from the magnetogram, the existence of such small-scale structures in the event under consideration is unlikely. The emission at the frequency close to the upper-hybrid frequency is polarized in the O-mode sense, and it is heavily damped when escaping the source; the emission that is generated due to the coalescence of two upper-hybrid waves is polarized in the X-mode sense, but the polarization degree is low at $\nu_p \gg \nu_B$.

A mechanism similar to the described one is proposed in the paper of LaBelle et al. (2003). The difference is that all the zebra stripes correspond to the same harmonic number s, and the discrete spectrum arises as a result of trapping the upper-hybrid waves with certain (resonance) wavelengths by the plasma microinhomogeneities (with sizes from several meters to several tens of meters). This model also requires an extended source with a size of about one thousand km. The parameters of the plasma and magnetic field inside the source, on the one hand, must be constant with high precision (in order to provide the narrow band emission); on the other hand, the emission frequency drift requires a synchronous change of the plasma and magnetic field parameters in the whole source, which is unlikely. The radio emission arises due to nonlinear transformation of upper-hybrid waves, and the high degrees of the X-mode polarization are difficult to obtain.

The coalescence of plasma waves with whistlers. In this model the zebra stripes are generated in different sources due to nonlinear coupling of upper-hybrid waves and whistlers, $\nu = \nu_{uh} + \nu_w$ (Chernov 1976, 1990). The whistler frequency ν_w does not exceed the electron cyclotron frequency, and the most effective generation (and the smallest damping) of whistlers occurs at $\nu_w \simeq 0.1\nu_B$. Therefore, the radio emission frequency is close to the plasma frequency (if $\nu_p \gg \nu_B$). Upper-hybrid waves are generated by an unstable electron beam in an extended region (with a size of about the dimensions of the coronal loop) and nonlinear transformation of the plasma oscillations into the radio emission (at the fundamental upper-hybrid frequency) forms the wide band background burst. Unlike upper-hybrid waves, whistlers are generated only in some local regions, due to the influence of the small-scale inhomogeneities or due to the nonlinear character of whistler interaction with an electron beam. Coalescence of whistlers with plasma waves results in the zebra pattern which, thus, is the reflection of the whistler generation spatial structure (several zebra stripes require the existence of several spatially separated sources). The interaction with whistlers results in the decrease of the upper-hybrid wave energy in the corresponding regions. As a consequence, the background burst intensity decreases and the absorption stripe is formed in the dynamic spectrum. The interval between adjacent bright and dark stripes in that model equals the whistler frequency, about $0.1\nu_B$. For the event under consideration this corresponds to a magnetic field strength of about 250−300 G.

As the emission frequency is very close to the plasma frequency in this model, the emission (both zebra pattern and background burst) should be polarized in the O-mode sense. This does not correspond to our observations. Moreover, it has been already noted that escaping the microwave emission with the frequency close to the plasma one requires either unrealistically high values of the plasma temperature or very sharp plasma density gradients. Thus, the coalescence of whistlers and upper-hybrid waves cannot account for the observed zebra pattern properties.

4.4.1. The interpretation of the absorption stripes

For the original dynamic spectrum we have detected a slight decrease of the background emission intensity (compared to the regions beyond the zebra pattern) between the zebra pattern bright stripes. This effect is best seen in the instant frequency spectra, and is less clear in Fig. 2. The absorption is observed only in the right-hand polarized emission, i.e. in the same polarization as the zebra pattern itself. It is evident that the mechanisms forming the emission and absorption stripes are closely connected.

In the model, explaining the zebra pattern by interaction of plasma waves and whistlers (Chernov 1976, 1990), the absorption bands arise due to decrease of the plasma wave energy in the sources of the bright zebra stripes. In the other models we need to consider a more complex source structure. Let us assume that the radio emission arises due to coalescence of Bernstein modes. The source of Bernstein modes is an electron beam with the radius r_{acc}. There is a transversal inhomogeneity of the plasma and magnetic field in the coronal loop, with the typical scale $L_\perp$. As a result, each loop point (with the $r < r_{acc}$) generates a discrete spectrum of the plasma waves and a discrete spectrum of the radio emission, but the inhomogeneity results in broadening the emission spectrum, and if $r_{acc}/L_\perp > \nu_B/\nu$, then the separate stripes merge and a continuous spectrum is formed. Next, the electron beam becomes more collimated: its radius decreases, so now $r_{acc} \ll L_\perp$, and the particle density n_{acc} increases (supposing that the energy flow is retained, $\pi r_{acc}^2 n_{acc} v_{acc} \simeq$ const.). In this case the emission from the loop periphery decreases, causing the decrease of the background burst intensity. In the loop center, on the contrary, the emission intensity increases, but this emission is now narrowband, with a clearly visible fine structure of a zebra pattern type. A similar effect is possible when the emission is generated on the double plasma resonance surfaces.

4.4.2. The interpretation of the frequency drift

In the dynamic spectrum of the zebra pattern which was observed after 06:06:10.3 UT, the U-form frequency drift is visible: the frequency of all the three bright stripes first decreases, and then increases. We believe that this behavior is caused by the heating and expansion of the local region in the magnetic loop, with subsequent cooling (Altyntsev et al. 2003). The local heating results in a decrease of the plasma density and (due to freezing-in of the magnetic field lines) in a decrease of the magnetic field, which is accompanied by a decrease of the emission frequency. Then, the heated region returns to the initial state and the emission frequency increases. The emission intensity decreases during the burst, and this indicates that the formation of the unstable electron distribution is connected with the heating process. The acceleration of particles is most effective during the heating phase. Note that the process of local heating naturally leads to a small source size (about one thousand km), and, therefore, all the zebra stripes will be generated in the same source (or in close sources).

5. Conclusion

We have presented observations of a solar microwave burst with the fine spectral structure of the zebra pattern type at the frequency of about 5.6 GHz. This is the first observation of a zebra pattern at such a high frequency. The zebra structure burst was observed by the instruments providing high spatial, temporal and spectral resolution. The main characteristics of the burst are:

The source size does not exceed 10 arcsec (7 thousand km). This value is related to the SSRT resolution and it is likely that the real source size is much smaller.

A spatial displacement between the sources of different zebra stripes has not been detected. Therefore, all the stripes are generated in the same spatial region (with a size of no more than several thousand km).

The degree of the zebra pattern circular polarization reaches 100%, and the sign corresponds to the extraordinary

wave (X-mode). The polarization degree of the background microwave burst is about 10%, with the same domination of the extraordinary wave.

The frequency interval between adjacent zebra stripes corresponds to the magnetic field strength 60−80 G in the source. Such values do not conflict with the background gyrosynchrotron emission parameters, and they allow us to explain the oscillation period of the magnetic loop.

The plasma density in the zebra pattern source can be estimated as 10^{11} cm^{-3}. This means that the emission frequency is close to the double plasma frequency.

The most probable mechanism of zebra pattern generation is nonlinear coupling of the harmonics of Bernstein modes.

Acknowledgements. The authors would like to thank Dr. M. Karlický for helpful comments.
This work was supported by the RFBR (grant numbers 02-02-39030 and 03-02-16229), by the Russia Department of Education (grant number E02-3.2-489), and by the *Integratsiya* project (I0208). Y.Y. is supported by MOST (G2000078403), NSFC (10225313 and 10333030) and CAS.

References

Altyntsev, A. T., Grechnev, V. V., Konovalov, S. K., et al. 1996, ApJ, 469, 976
Altyntsev, A. T., Kuznetsov, A. A., Meshalkina, N. S., & Yihua Yan 2003, A&A, 411, 263
Aschwanden, M. J., De Pontieu, B., Schrijver, C. J., & Title, A. M. 2002, Sol. Phys., 206, 99
Aurass, H., Klein, K.-L., Zlotnik, E. Ya., & Zaitsev, V. V. 2003, A&A, 410, 1001
Benz, A. O., Magun, A., Stehling, W., & Su, H. 1992, Sol. Phys., 141, 335
Chernov, G. P. 1976, Soviet Astron., 20, 582
Chernov, G. P. 1990, Sol. Phys., 130, 75
Chernov, G. P., & Zlobec, P. 1995, Sol. Phys., 160, 79
Chernov, G. P., Korolev, O. S., & Markeev, A. K. 1975, Sol. Phys., 44, 435
Chernov, G. P., Klein, K.-L., Zlobec, P., & Aurass, H. 1994, Sol. Phys., 155, 373
Chernov, G. P., Yasnov, L. V., Yan, Y. H., & Fu, Q. J. 2001, Chin. J. Astron. Astrophys., 1, 525
Chernov, G. P., Yan, Y. H., & Fu, Q. J. 2003, A&A, 406, 1071
Chiuderi, C., Giachetti, R., & Rosenberg, H. 1973, Sol. Phys., 33, 225
Dulk, G. A. 1985, ARA&A, 23, 169
Fleishman, G. D., & Melnikov, V. F. 1998, Uspekhi Fiz. Nauk, 168, 1265 (Engl. translation: Physics-Uspekhi, 41, 1157)
Fu, Q., Qin, Z., Ji, H., & Pei, L. 1995, Sol. Phys., 160, 97
Grechnev, V. V., Lesovoi, S. V., Smolkov, G. Ya., et al. 2003, Sol. Phys., 216, 239
Güdel, M. 1990, A&A, 239, L1
Ji, H., Fu, Q., Liu, Y., et al. 2003, Sol. Phys., 213, 359
Haruki, T., & Sakai, J.-I. 2001, ApJ, 552, L175
Kuijpers, J. 1975, A&A, 40, 405
LaBelle, J., Treumann, R. A., Yoon, P. H., & Karlicky, M. 2003, ApJ, 593, 1195
Ledenev, V. G., Karlický, M., Yan, Y., & Fu, Q. 2001, Sol. Phys., 20, 71
Mollwo, L., & Sauer, K. 1977, Sol. Phys., 51, 435
Rosenberg, H. 1972, Sol. Phys., 25, 188
Rudenko, G. V., Altyntsev, A. T., & Lubyshev, B. I. 1998, JOSO Annual report '97, Astronomical Institute (Slovakia: Tatranska Lomnica), 94
Rudenko, G. V., & Grechnev, V. V. 1999, ASP Conf. Ser., Astronomical Data Analysis Software and Systems VIII, ed. D. M. Mehringer, R. L. Plante, & D. A. Roberts (San Francisco: ASP), 172, 421
Sawant, H. S., Karlický, M., Fernandes, F. C. R., & Cecatto, J. R. 2002, A&A, 396, 1015
Schrijver, C. J., Aschwanden, M. J., & Title, A. M. 2002, Sol. Phys., 206, 69
Smolkov, G. Y., Pistolkors, A. A., Treskov, T. A., Krissinel, B. B., & Putilov, V. A. 1986, Ap&SS, 119, 1
Willes, A. J. 1999, Sol. Phys., 186, 319
Willes, A. J., & Robinson, P. A. 1996, ApJ, 467, 465
Winglee, R. M., & Dulk, G. A. 1986, ApJ, 307, 808
Yasnov, L. V., & Karlický, M. 2004, Sol. Phys., 219, 289
Zaitsev, V. V., & Stepanov, A. V. 1983, Sol. Phys., 88, 297
Zheleznyakov, V. V., & Zlotnik, E. Ya. 1975a, Sol. Phys., 43, 431
Zheleznyakov, V. V., & Zlotnik, E. Ya. 1975b, Sol. Phys., 44, 461
Zlobec, P., Messerotti, M., Comari, M., Li, H.-W., & Barry, M. B. 1987, Sol. Phys., 114, 375
Zlotnik, E. Ya. 1977, AZh, 54, 1309
Zlotnik, E. Ya. 1981, A&A, 101, 250
Zlotnik, E. Ya., Zaitsev, V. V., Aurass, H., Mann, G., & Hofmann, A. 2003, A&A, 410, 1011